

Lifetime measurements in the ground-state band in  $^{104}\text{Pd}$ 

M. Droste<sup>1,\*</sup>, A. Blazhev<sup>1</sup>, P. Reiter<sup>1</sup>, K. Arnsward<sup>1</sup>, M. Beckers<sup>1</sup>, C. Fransen<sup>1</sup>, R. Hetzenegger<sup>1</sup>, R. Hirsch<sup>1</sup>, L. Kaya<sup>1</sup>, L. Knafla<sup>1</sup>, L. Lewandowski<sup>1</sup>, C. Müller-Gatermann<sup>1</sup>, P. Petkov<sup>2</sup>, D. Rosiak<sup>1</sup>, M. Seidlitz<sup>1</sup>, B. Siebeck<sup>1</sup>, A. Vogt<sup>1</sup>, N. Warr<sup>1</sup> and K. Wolf<sup>1</sup>

<sup>1</sup>*Institut für Kernphysik, Universität zu Köln, D-50937 Köln, Germany*

<sup>2</sup>*“Horia Hulubei” National Institute for Physics and Nuclear Engineering, R-76900 Bucharest-Măgurele, Romania*



(Received 29 April 2022; accepted 8 August 2022; published 26 August 2022)

Lifetimes and reduced transition probabilities were determined in the ground-state band in  $^{104}\text{Pd}$  up to the  $12^+$  state employing the recoil distance Doppler-shift method. Excited states were populated via the fusion-evaporation reaction  $^{96}\text{Zr}(^{12}\text{C}, 4n)^{104}\text{Pd}$  at 55 MeV. The  $B(E2; 2_1^+ \rightarrow 0_{\text{g.s.}}^+)$  value deviates from previous evaluated values obtained by Coulomb excitation and electron scattering. The transition strengths for higher-lying states were obtained for the first time, closing a gap in the medium-mass Pd isotope chain. Large-scale shell-model calculations were performed employing the SR88MHJM Hamiltonian along the isotope chain  $^{96}\text{--}^{106}\text{Pd}$  for even-even nuclei and for high-spin states up to  $26^+$  in  $^{104}\text{Pd}$ .

DOI: [10.1103/PhysRevC.106.024329](https://doi.org/10.1103/PhysRevC.106.024329)

## I. INTRODUCTION

The nucleus  $^{104}_{46}\text{Pd}_{58}$  is four protons and eight neutrons away from the nearest double-shell closure at  $^{100}\text{Sn}$ . Nuclei in this region of the Segrè chart are generally considered as good examples for vibrator nuclei, observable via characteristic level schemes of the first excited states [1]. Especially in  $^{104}\text{Pd}$ , excitation energies of the  $2_2^+$ ,  $0_2^+$ , and  $4_1^+$  states are very close within a range of only 20 keV. Transition strengths in the palladium isotope chain starting from the  $N = 52$  isotope  $^{98}\text{Pd}$  up to the  $N = 60$  isotope  $^{106}\text{Pd}$  have been investigated recently in direct [2–6] and indirect [7] lifetime measurements. As an outcome of these studies, the vibrational character of the Pd isotopes has been questioned indicating a rather rotational behavior.

Experimental data on the electromagnetic structure of  $^{104}\text{Pd}$  are surprisingly scarce in contrast to neighboring, heavier, even-even isotopes [8]. Model-independent approaches like precise lifetime measurements are needed to determine reduced transition strengths in  $^{104}\text{Pd}$  especially for the first excited  $2^+$  state. In the past,  $B(E2; 2_1^+ \rightarrow 0_{\text{g.s.}}^+)$  values were determined from Coulomb excitation (Coulx) experiments with proton and  $^4\text{He}$  beams [8]. Two pioneering Coulex experiments carried out by Temmer *et al.* [9] and Stelson *et al.* [10] in 1956 and 1958, respectively, based on comparable beam energies investigated various medium-mass even-even isotopes. The data analysis was based on the semiclassical theory of multiple Coulex developed by Alder and Winther [11]. Despite the similarity of the experimental approach, transition strengths differed by a factor of two not only for  $^{104}\text{Pd}$  but also for other isotopes, such as  $^{110}\text{Pd}$ .

An improved Coulex experiment utilizing a  $^{16}\text{O}$  beam and an analysis which partially used the GOSIA code [12,13] was

performed by Christy *et al.* [14] in 1970. However, matrix elements were mainly extracted with the Winther-de Boer code [15] and unknown matrix elements related to higher-lying states were adopted from other medium-mass Pd isotopes. In addition an electron scattering experiment was performed by Wesseling *et al.* in 1990 [16].

The measurements by Luontama *et al.* [17] exploited protons for an investigation of transition strengths in  $^{102,104}\text{Pd}$ . The results were normalized to the  $B(E2; 2_1^+ \rightarrow 0_{\text{g.s.}}^+)$  value of  $^{104}\text{Pd}$ , which was taken from Ref. [12]. Surprisingly, lifetimes and transition strengths of medium-spin states above the  $4_1^+$  state in  $^{104}\text{Pd}$  are unknown, a unique gap along the medium-mass palladium isotope chain. The  $B(E2; 4_1^+ \rightarrow 2_1^+)$  value has so far only been measured by Luontama *et al.*

Very short lived high-spin ( $J_1^+ \geq 16_1^+$ ) states in  $^{104}\text{Pd}$  were subject to lifetime measurements employing the Doppler-shift attenuation Method (DSAM) in order to search for and to investigate antimagnetic rotational bands [18]. Antimagnetic rotation is a mechanism for the generation of high-spin states and was first proposed by Frauendorf [19]. This excitation mechanism is based on the  $M1$  shears mode, where the total angular momentum is generated by the angular momenta of the valence protons and neutrons. The single-particle configuration of  $^{104}\text{Pd}$  allows for the perpendicular coupling of these two angular momentum vectors [18]. The latest DSAM experiments were carried out by Majumder *et al.* [20] in 2020, exploring negative-parity high-spin states in addition to positive-parity yrast states. High-spin states were previously also assigned by Sohler *et al.* [21].

Recently, lifetime measurements were performed by Ivanova *et al.* [22] in the odd-even Pd isotopes  $^{99\text{--}105}\text{Pd}$  using the fast-timing technique as well as the recoil distance Doppler-shift (RDDS) method for  $^{103}\text{Pd}$ .

Due to the low excitation energy of the  $2_1^+$  state and its enhanced collectivity, the stable midshell nucleus  $^{104}\text{Pd}$  is frequently used as a target material in Coulex experiments at

\*Corresponding author: [mdroste@ikp.uni-koeln.de](mailto:mdroste@ikp.uni-koeln.de)

radioactive ion-beam facilities. For these experiments precise knowledge of the transition probabilities and the correlated quadrupole moments of the target material is mandatory.

The nuclear structure in palladium isotopes has been a subject to various theoretical approaches. IBM-1 and IBM-2 calculations reproduce excitation energies of low-spin states but show discrepancies in transition strengths [23,24]. Shell-model (SM) calculations based on a  $^{88}\text{Sr}$  core were performed in the lighter Pd isotopes  $^{100,102}\text{Pd}$  by Radeck *et al.* [4] yielding a good description of  $B(E2)$  values of positive-parity ground-state band transitions. Theoretical investigations in  $^{104}\text{Pd}$  were subject to studies by Zhang *et al.* [25] examining the antimagnetic rotational band using a particle-number-conserving method based on the cranked shell model.

Large-scale shell-model (LSSM) calculations in the  $\pi(2p_{1/2}, 1g_{9/2})\nu(2d_{5/2}, 1g_{7/2}, 2d_{3/2}, 3s_{1/2}, 1h_{1/2})$  model space employing the  $M$ -scheme code KSHELL [26] became tractable for heavier Pd isotopes due to advances in computational performance and by updated shell-model codes. The SR88MHJM [27–32] interaction calculations are expected to elucidate the emergence and nature of the increasing collectivity in the Pd isotopes and they are the subject of this publication.

A direct lifetime measurement in the ground-state band of  $^{104}\text{Pd}$  up to the  $12^+$  state was performed at the Institute of Nuclear Physics of the University of Cologne employing the RDDS method. The measured  $B(E2; (J+2)_1^+ \rightarrow J_1^+)$  values are compared with new LSSM calculations. The paper is organized in the following way: Experimental details are outlined in Sec. II. The lifetime analysis is subsequently described in Sec. III and its results are presented for the individual states in Sec. IV. A detailed comparison with results of new shell-model calculations is given in Sec. V, followed by a brief summary.

## II. EXPERIMENTAL DETAILS

The lifetime experiment was performed at the FN tandem accelerator of the Institute for Nuclear Physics, University of Cologne. A combined setup of high-purity germanium (HPGe) detectors and the Cologne coincidence-plunger device was exploited. Excited states in the nucleus of interest were populated by the fusion-evaporation reaction  $^{96}\text{Zr}(^{12}\text{C}, 4n)^{104}\text{Pd}$  with an anticipated yield of 85% of the total fusion cross section at the beam energy of 55 MeV. The  $^{12}\text{C}$  beam was extracted from the Cologne ion sputter source and impinged onto the  $1\text{ mg/cm}^2$  Zr target, which was enriched to 72.47%  $^{96}\text{Zr}$ . Recoiling nuclei left the target with 0.87(4)% of the speed of light and were finally stopped in a  $3.7\text{-mg/cm}^2$ -thick  $^{197}\text{Au}$  foil.

During the experiment data were recorded for 12 different target-to-stopper distances, i.e., different flight times of the recoiling nuclei. The distances covered a range from 26.1 to 426.7  $\mu\text{m}$ . The distances were measured with an accuracy better than 1%. Beam-induced variations of the distance caused, e.g., by the thermal expansion of the target, were compensated by a feedback system employing a piezoelectric linear motor.

Emitted  $\gamma$  rays were detected by 12 HPGe detectors positioned in rings centered at angles of  $\theta_0 = 0^\circ$  (one detector),  $\theta_1 = 45^\circ$  (six detectors), and  $\theta_2 = 142.3^\circ$  (five detectors) with

respect to the beam axis. A hardware coincidence-trigger condition was used in order to suppress single  $\gamma$ -ray events. Coincident  $\gamma$ -ray events were sorted into  $\gamma\gamma$  matrices for each target-to-stopper distance. Two groups are defined by the two individual detector rings of same  $\theta$  values. Four correlation groups are defined (“1\_1,” “1\_2,” “2\_1,” “2\_2,” with 1\_2 being the abbreviation for coincidence data which require  $\gamma$ -rays detected in ring 2 at  $\theta_2$   $142.3^\circ$  with respect to the beam axis and gated spectra are analysed for detectors in ring 1 under forward angles). A projection of the  $\gamma\gamma$  matrix summed up for all measured distances is shown in Fig. 1 for the detector ring 1. In addition to transitions in  $^{104}\text{Pd}$ , only few transitions have to be assigned to other evaporation residues, as  $^{104}\text{Pd}$  was dominantly populated in the reaction (see Fig. 1).

## III. DATA ANALYSIS

The lifetime analysis is based on the RDDS technique and the differential decay-curve method (DDCM), both described in detail in Refs. [33,34]. Due to the high production yield of the recoiling nuclei of interest, the DDCM was utilized in the  $\gamma\gamma$ -coincidence mode. Employing gates on the Doppler-shifted component of feeding transitions of the state of interest, lifetimes are determined by analyzing the intensity ratio of the Doppler-shifted (SH) and unshifted (US) components of the depopulating transition.

$$\tau(x) = \frac{I_{\text{US}}(x)}{\frac{d}{dx}I_{\text{SH}}(x)} \cdot \frac{1}{v}. \quad (1)$$

The lifetime analysis employing this method is based on detailed knowledge of the intensity distribution of shifted and unshifted components for different target-to-stopper distances. The  $\gamma$ -ray intensities are normalized for the runs of different target-to-stopper distances. Independent lifetimes are determined for each target-to-stopper distance  $i$ , corresponding to a certain flight time  $t_i$ , as well as for the four detector correlation groups. Equation (1) is employed to calculate the lifetime for each individual distance. The final lifetime  $\tau$  is deduced from the weighted mean of the different lifetimes  $\tau_i(x)$  including distances in the sensitive range as defined in Ref. [33]. The statistical uncertainty of the lifetime value is dominated by the distribution of the single  $\tau_i$  values. Systematic errors of the lifetime arise mainly from the uncertainty of the recoil velocity, which is inversely included in the lifetime value [35].

The velocity is deduced from the angle-dependent Doppler shift observed for each detector-ring combination. The opening angle  $\Delta\theta = 3^\circ$  of the individual Ge detectors corresponds to  $\Delta\beta/\beta = 0.05$ . In addition, the momentum distribution of the reaction products and their energy loss in the target cause a velocity distribution of the recoiling nuclei after the target, i.e., a range of flight times between target and stopper foil. Thus, nuclei with higher velocities are stopped earlier especially for the shortest distance and the velocity distribution of nuclei that emitted a  $\gamma$  ray in flight, depends on the target-to-stopper distance. A correction was applied in order to account for the effect of different mean flight times as a function of target-to-stopper distances. The correction is further described in Refs. [35,36]. The target-to-stopper distances were

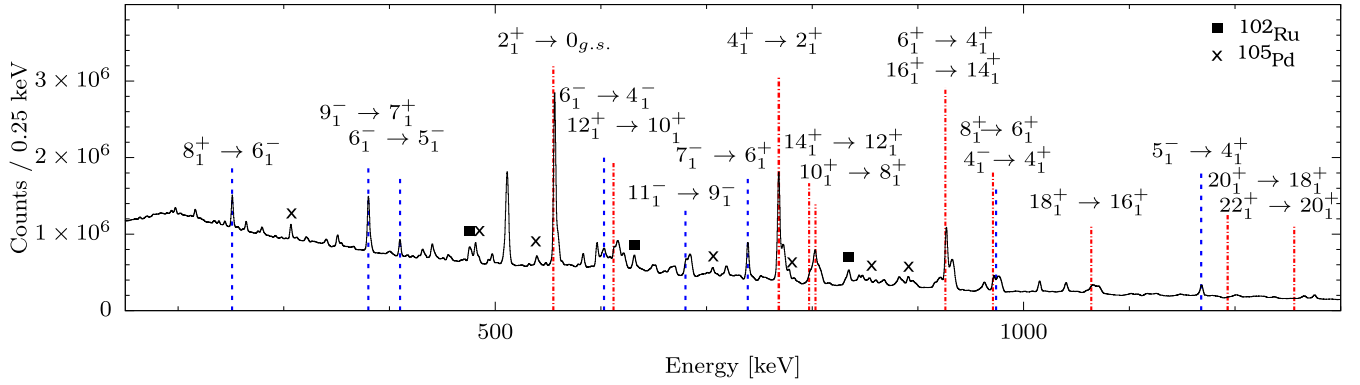


FIG. 1.  $\gamma$ -ray energy spectrum for the detector ring at  $45^\circ$  with respect to the beam axis summed for all plunger distances. Marked  $\gamma$  rays are assigned to (red) positive- and (blue) negative-parity states in  $^{104}\text{Pd}$ , respectively. The labels indicate the energies from decays at rest, Doppler-shifted  $\gamma$  rays are partially visible.  $\gamma$  rays from  $^{102}\text{Ru}$  and  $^{105}\text{Pd}$  are marked with filled squares and crosses, respectively.

measured with a high precision of  $\Delta x \leq 0.4 \mu\text{m}$  in the sensitive range. Its contribution to the total uncertainty of  $\tau$  was neglected.

For long lifetimes  $\tau > 3.5$  ps the assumption was made that all excited states decay either during flight in vacuum and are detected Doppler-shifted, or the  $\gamma$  rays are emitted at rest in the stopper foil. The slowing-down processes in the target- and stopper foils were neglected. However, in case of a short lifetime comparable to the slowing-down time of the recoiling nucleus, Doppler-shift attenuation can be observed in the energy range between the shifted and unshifted peaks. In order to correct for this effect, gated spectra were simulated with a Monte Carlo calculation taking into account the kinematics of the recoiling nuclei and the material properties of the target and stopper foils. These spectra are analysed in the same way as the experimental spectra, without considering attenuation effects. A correction factor  $c(\tau)$  as a function of the lifetime was determined and experimental lifetimes are multiplied with the corresponding  $c(\tau)$  value. The method is explained in detail in Refs. [37–39]. As an example, the correction curve for the lifetime analysis of the  $4^+$  state is shown in Fig. 2.

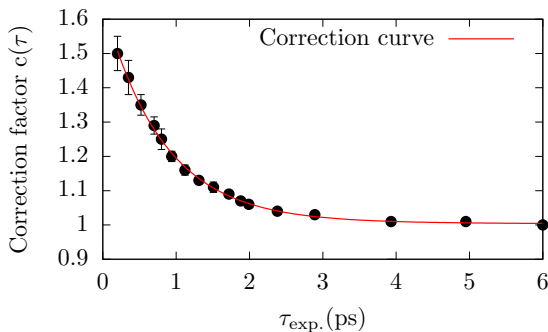


FIG. 2. Correction factors  $c(\tau)$  are deduced by comparing 17 simulated lifetimes with resulting analysed lifetime values and are shown for the  $4_1^+$  state in  $^{104}\text{Pd}$ . An exponential function is fitted to the data points and is shown in red.

## IV. RESULTS

The considerable statistics of the transitions within the yrast band in  $^{104}\text{Pd}$  allowed lifetime determination up to the  $12^+$  state. The lifetime analyses of the individual states are described below and the results are summarized in Table I.

### A. $2_1^+$ state at 556 keV

For the lifetime analysis of the  $2_1^+$  state narrow gates on the shifted component of the direct feeding  $4_1^+ \rightarrow 2_1^+$  transition at 767 keV were employed. Gated  $\gamma$ -ray spectra recorded at forward angles with gates on the same ring are shown in Figs. 3(a1)–3(a6). The evolution of the peak intensities in the Doppler-shifted and unshifted components with increasing flight distance of the  $^{104}\text{Pd}$  recoils is demonstrated. Two Gaussian peaks were fitted to the measured peaks indicated by red lines. Energy resolution data from the  $^{226}\text{Ra}$  calibration source measurement were used to constrain the peak width of the unshifted component. By gating on the shifted component of the feeding transition, the lifetime is deduced for every distance according to Eq. (1). The  $\tau$  curve of the  $2_1^+$  state and the corresponding  $\gamma$ -ray intensities for the detector ring at  $45^\circ$  and a gate on the same ring are presented in Figs. 4(a)–4(c). Second-order polynomial functions were fitted piecewise to the shifted intensity data points [Fig. 4(c)]. The derivative is fitted to the unshifted data points Fig. 4(b). The lifetime was determined from the weighted mean of each distance shown in Fig. 4(a) together with its  $1\sigma$  deviation. The weighted mean value of four independent lifetimes are deduced from the four different detector-ring combinations. The final lifetime value results in  $\tau(2_1^+) = 16.48(12)_{\text{stat.}}(87)_{\text{sys.}}$  ps. The systematic error arises from uncertainties in detector positions. The newly determined lifetime of the  $2_1^+$  state corresponds to a reduced transition probability of  $B(E2; 2_1^+ \rightarrow 0_{\text{g.s.}}^+) = 31.7(16)$  W.u., while the adopted lifetime is  $\tau = 14.48(40)$  ps and  $B(E2; 2_1^+ \rightarrow 0_{\text{g.s.}}^+) = 36.4(10)$  W.u. [8].

### B. $4_1^+$ state at 1324 keV

The analysis of the  $4_1^+$  state at 1324 keV is hampered by two issues. First, the feeding  $\gamma$ -ray transition  $6_1^+ \rightarrow 4_1^+$  of the

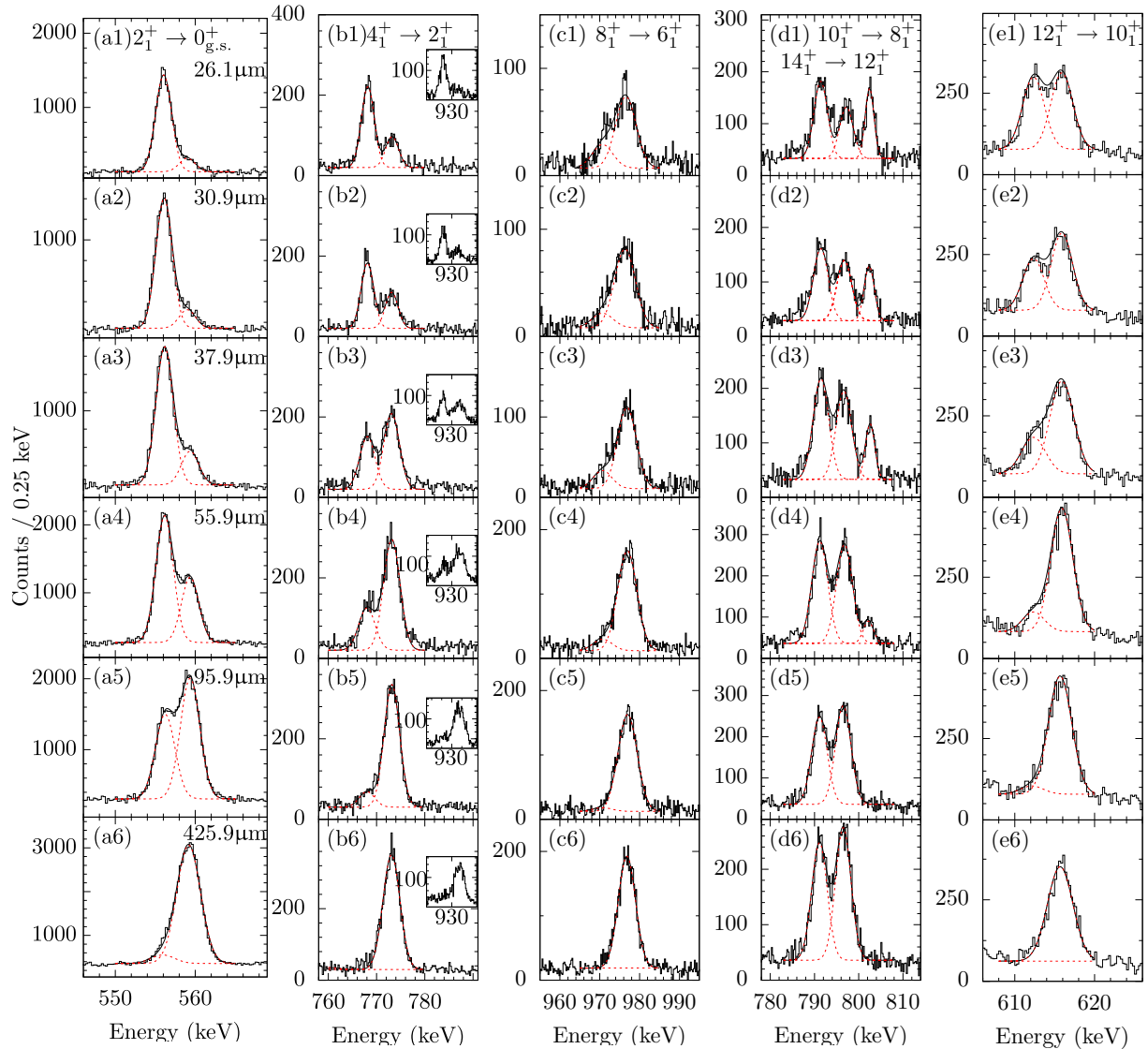


FIG. 3.  $\gamma$ -ray spectra of the yrast band in  $^{104}\text{Pd}$  for the decays of the  $2_1^+$ ,  $4_1^+$ ,  $8_1^+$ ,  $10_1^+$ , and  $12_1^+$  states [(a)–(e)]. Spectra are produced by employing gates on the Doppler-shifted component of the direct feeding transitions of the yrast band. Spectra of  $2_1^+$ ,  $4_1^+$ ,  $8_1^+$ , and  $12_1^+$  decays are shown for six different target-to-stopper distances at a forward angle of  $45^\circ$ . The spectra for the  $10_1^+ \rightarrow 8_1^+$  transition are shown for backward angles due to the closely contaminating  $14_1^+ \rightarrow 12_1^+$  transition observed for forward angles. The transition is visible at higher energies in the spectra (d1)–(d4). The fits to the unshifted and Doppler-shifted components are indicated by dashed red lines. The lifetime analysis of the  $4_1^+$  state requires additional information on intensities of direct feeding transition in gated spectra due to a doublet in the positive-parity ground-state band.

$4_1^+$  state is emitted from the short-lived  $6_1^+$  state. Other feeding transitions, for example from the negative-parity band states which decay directly into the  $4_1^+$  state are very long lived, and no shifted component was observed even for the largest distances. The feeding  $6_1^+ \rightarrow 4_1^+$  transition has the same energy as the higher-lying  $16_1^+ \rightarrow 14_1^+$  ground-state band transition at  $E_\gamma(16_1^+ \rightarrow 14_1^+) = E_\gamma(6_1^+ \rightarrow 4_1^+) = 926.2$  keV. Hence, in the gated spectrum a superposition of these direct and indirect gates emerges [see Figs. 3(b1)–3(b6)]. In the gated spectrum, a peak is visible in the energy range of 925–933 keV [see inset panels Figs. 3(b1)–3(b6)]. By gating also on the

higher-lying  $16_1^+ \rightarrow 14_1^+$  doublet transition the shifted and unshifted component of the  $6_1^+ \rightarrow 4_1^+$  transition appears. This allows a background correction of the stopped component of the  $4_1^+ \rightarrow 2_1^+$  transition. Second, its small lifetime approaches the time limit which can be studied by RDDS experiments. For the lifetime of  $\tau = 1.90(5)_{\text{stat.}}(12)_{\text{sys.}}$  ps the DSA correction with a factor of  $c(\tau) = 1.08(1)$  was applied. The correction curve is shown in Fig. 2. The lifetime analysis for gate and analysis of the forward detector ring is shown in Figs. 4(d)–4(f). The final determined lifetime of the  $4_1^+$  state is  $\tau(4_1^+) = 2.08(20)$  ps.

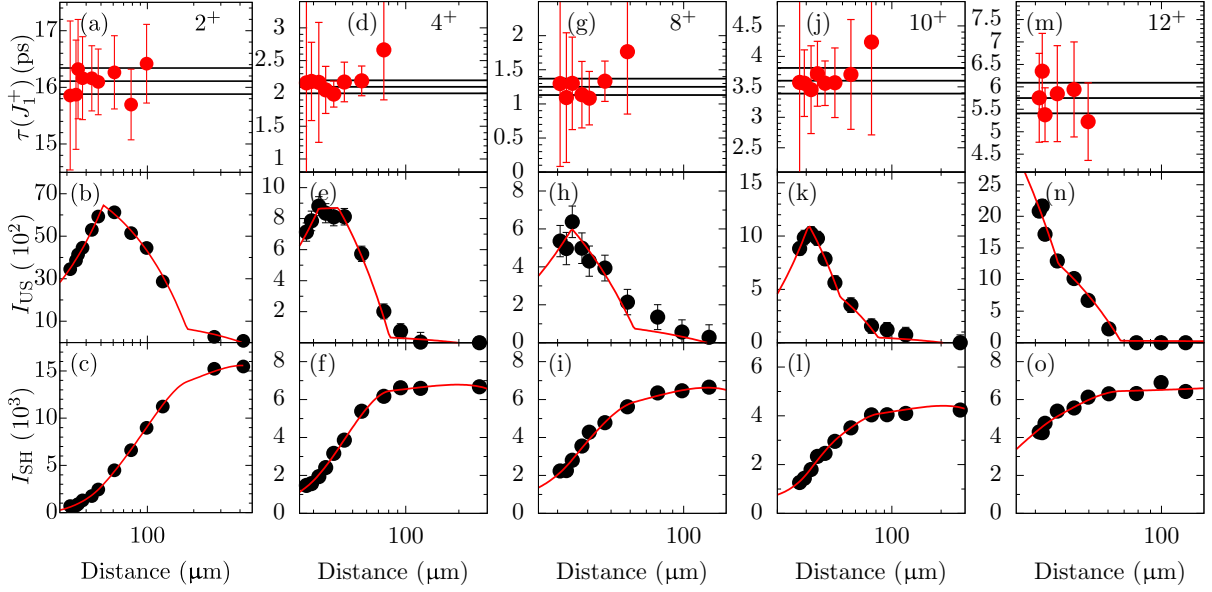


FIG. 4.  $\tau$  curves of the (a)  $2_1^+$  (d)  $4_1^+$  (g)  $8_1^+$  (j)  $10_1^+$ , and (m)  $12_1^+$  states in  $^{104}\text{Pd}$  are shown exemplary for one analysis gate combination. Lifetimes and  $\gamma$ -ray intensities are presented in dependence of the target-to-stopper distance. The black solid lines indicate the weighted mean value of the individual lifetimes; surrounding lines mark the statistical uncertainty. Furthermore, the unshifted [(b), (e), (h), (k), and (n)] and shifted [(c), (f), (i), (l), and (o)] intensities of the depopulating transitions are shown. The polynomial fit function to the given intensities is presented as a dashed red line. Note the logarithmic distance scale.

### C. $6_1^+$ state at 2250 keV

The lifetime analysis of the  $6_1^+$  state is also affected by the energy doublet of the  $6_1^+ \rightarrow 4_1^+$  transition and the  $16_1^+ \rightarrow 14_1^+$  transition, both with an energy of  $E_\gamma = 926.2$  keV. A gate was set on the Doppler-shifted component of the feeding  $8_1^+ \rightarrow 6_1^+$  transition at 971 keV. Since the gate was placed on the shifted component of a lower-lying state relative to the  $16_1^+$  state, the measured component of the  $16_1^+ \rightarrow 14_1^+$  transition is completely Doppler shifted in energy. In the resulting spectrum, the Doppler-shifted component of the 926.2-keV peak contains the sum of the shifted components of the  $6_1^+ \rightarrow 4_1^+$  and  $16_1^+ \rightarrow 14_1^+$  transitions. According to Eq. (1), the lifetime is inversely proportional to the change in the Doppler-shifted component of the state of interest relative to the target-to-stopper distance. Accurate subtraction

of the interfering  $16_1^+ \rightarrow 14_1^+$  component is not possible. Two limits were considered for an evaluation of the lifetime. First, the impact of the  $16_1^+ \rightarrow 14_1^+$  transition was disregarded and a lower limit of the lifetime was deduced. Second, the highest possible contribution to the intensity of the shifted component was estimated and used for an upper lifetime limit. For the estimate the intensity ratio between the higher-lying  $8_1^+ \rightarrow 6_1^+$  and lower-lying  $14_1^+ \rightarrow 12_1^+$  yrast transitions was determined. Taking into account that measured yields from consecutive states within the yrast band are increasing with decreasing angular momentum, the transition intensity ratio of  $I(8_1^+ \rightarrow 6_1^+)/I(14_1^+ \rightarrow 12_1^+)$  has to be smaller than the ratio of the  $6_1^+ \rightarrow 4_1^+$  and  $16_1^+ \rightarrow 14_1^+$  transitions. An upper limit for the possible contribution by the Doppler-shifted component of the  $16_1^+ \rightarrow 14_1^+$  transition

TABLE I. Resulting lifetimes in the positive-parity ground-state band are summarized up to the  $12_1^+$  state. Experimental transition energies and transition strengths of low-spin states expressed in  $B(E2)$  values are compared with results of LSSM calculations employing the SR88MHJM interaction. Branching ratios of the  $10_1^+ \rightarrow 8_1^+$  and  $12_1^+ \rightarrow 10_1^+$  transition were adopted from Ref. [21]. Additionally, results of a modified interaction are shown, marked with an asterisk.

$J_1^+$	$E(J_1^+)$	$\tau(J_1^+)$ (ps)		$E_\gamma[J_1^+ \rightarrow (J-2)_1^+]$ (keV)			$B[E2; J_1^+ \rightarrow (J-2)_1^+]$ ( $e^2 \text{fm}^4$ )		
		Expt.	Expt.	Expt.	SR88MHJM	SR88MHJM*	Expt.	SR88MHJM	SR88MHJM*
$2_1^+$	556	16.48(88)	556	629	637	$927_{-48}^{+53}$	947	956	
$4_1^+$	1324	2.08(20)	768	810	817	$1469_{-129}^{+156}$	1376	1391	
$6_1^+$	2250	1.15(45)	926	916	917	$1030_{-300}^{+600}$	1518	1539	
$8_1^+$	3221	1.40(16)	971	927	912	$670_{-65}^{+80}$	1135	1155	
$10_1^+$	4023	3.55(27)	803	1007	929	$620_{-44}^{+51}$	1311	471	
$12_1^+$	4635	5.90(40)	612	674	462	$1520_{-100}^{+110}$	68	1500	

was determined and subtracted from the shifted component visible in the spectrum. The lifetime value of the  $6_1^+$  state was taken from the weighted mean of these two limits  $\tau(6_1^+) = 1.15(45)$  ps. The limits define the systematic error.

#### D. $8_1^+$ state at 3221 keV

Intensities of the  $8_1^+ \rightarrow 6_1^+$  transition are shown for six different target-to-stopper distances in Figs. 3(c1)–3(c6). The lifetime analysis is presented for a gate and analysis of the forward angle detector ring in Figs. 4(g)–4(i). Only forward angle gating was used for the lifetime analysis of the  $8_1^+$  state due to a contamination caused by two coincident  $\gamma$ -ray transitions in  $^{104}\text{Pd}$  with  $E_\gamma(14_1^+ \rightarrow 12_1^+) = 797$  keV and  $E_\gamma(10_1^+ \rightarrow 8_1^+) = 803$  keV. A lifetime value of  $\tau(8_1^+) = 1.26(10)_{\text{stat.}}(9)_{\text{sys.}}$  ps was multiplied by a DSA correction factor of  $c(\tau) = 1.12$ . A final lifetime value of  $\tau(8_1^+) = 1.40(12)_{\text{stat.}}(11)_{\text{sys.}}$  ps is obtained.

#### E. $10_1^+$ state at 4023 keV

The lifetime of the  $10_1^+$  state is deduced by gating on the shifted component of the direct feeding  $12_1^+ \rightarrow 10_1^+$  transition. The backward detector ring was analysed in order to avoid contaminations from the close-by energies of the  $10_1^+ \rightarrow 8_1^+$  and  $14_1^+ \rightarrow 12_1^+$  transitions. The line-shape evolution is shown in Figs. 3(d1)–3(d6). Only the Doppler-shifted part of the contaminating transition is visible since the gate was placed on the shifted component of a lower-lying state relative to the contaminant. Thus, the contaminant could be taken into account in the analysis and showed no influence on the determination of the lifetime under backward angles. The final lifetime value is determined by the mean lifetime value, deduced for eight distances and for two detector ring combinations to  $\tau(10_1^+) = 3.55(12)_{\text{stat.}}(24)_{\text{sys.}}$  ps. The analysis for a correlation group with gate and analysis under backward angles is shown in Figs. 4(j)–4(l).

#### F. $12_1^+$ state at 4635 keV

Independent lifetimes of the  $12_1^+$  state were determined by gating on the backward detector angles due to the small energy difference between the direct feeder and the lower lying transition in the ground-state band. Gated spectra are shown in Figs. 3(e1)–3(e6) for the forward detector ring. The corresponding lifetime analysis is presented in Figs. 4(m)–4(o). The weighted mean of the two lifetimes deduced for the detector ring at forward and backwards angle yields a lifetime of  $\tau(12_1^+) = 5.90(20)_{\text{stat.}}(35)_{\text{sys.}}$  ps.

### V. SHELL-MODEL CALCULATIONS

The experimentally obtained lifetimes and corresponding reduced transition probabilities in  $^{104}\text{Pd}$  are compared with shell-model theory. For this purpose shell-model calculations were performed using the *M*-scheme code KSHHELL [26]. The SR88MHJM interaction [27–32] is employed with an inert  $^{88}\text{Sr}$  core including orbitals up to  $Z = 50$  and  $N = 82$ . The model space comprises valence neutrons in the  $\nu(2d_{5/2}, 1g_{7/2},$

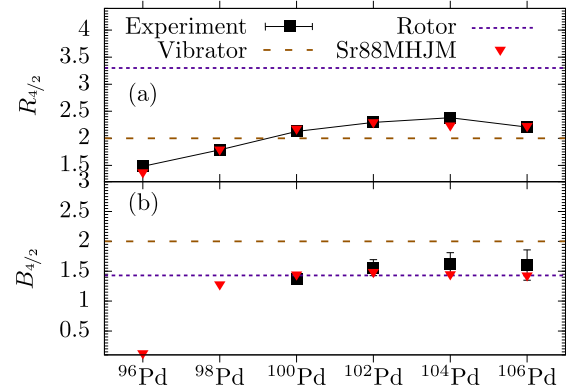


FIG. 5. Experimental and calculated ratios of  $4_1^+$  and  $2_1^+$  (a) excitation energies and (b)  $B(E2)$  values.

$2d_{3/2}, 3s_{1/2}, 1h_{11/2}$ ) orbitals and protons in the  $\pi(2p_{1/2}, 1g_{9/2})$  orbitals. The SR88MHJM interaction is employed for isotopes south-east from  $^{100}\text{Sn}$  and is based on the CD-Bonn potential with renormalization of the G matrix. The G matrix is derived from a nucleon-nucleon (*NN*) potential with core-polarization correction and adjusted to experimental data [27,28]. Single-particle energies (SPE) are inferred from  $^{88}\text{Sr}$  one-proton and one-neutron neighbors and monopole corrections are applied to reproduce single-neutron particle energies and single-proton hole energies in tin isotopes and two-body matrix elements were adjusted to optimize the agreement with experimental energies in the tin isotopes [27,29,32]. Effective charges  $e_\nu = 1.0e$  and  $e_\pi = 1.7e$  for neutrons and protons, respectively, as well as effective spin g factors  $g_{\text{eff.}}^s = 0.7 g_{\text{free}}^s$  were used. Shell-model calculations with this interaction have been performed for odd cadmium isotopes between  $^{101}\text{Cd}$  and  $^{111}\text{Cd}$ ; the values for effective charges and g factors reproduce experimental  $B(E2)$  values and magnetic moments in the neighboring Cd isotopes [29,31].

#### A. Shell-model calculations for $^{96-106}\text{Pd}$

Shell-model calculations with the SR88MHJM interaction span the Pd isotope chain, starting from the  $N = 50$  shell closure up to the  $N = 60$  isotope  $^{106}\text{Pd}$ . As a first result, the experimental and calculated ratios of  $4_1^+$  and  $2_1^+$  excitation energies ( $R_{4/2}$ ) and transition strengths ( $B_{4/2}$ ) are compared for six isotopes along the  $Z = 46$  isotope chain. The  $R_{4/2} = E(4_1^+)/E(2_1^+)$  ratio is typically used as an indicator for nuclear shape properties. Values below two correspond to excitations related to states of single-particle character, while higher values of  $R_{4/2}$  correspond to states which show collective properties. The exact value of two corresponds to the expected ratio for a harmonic vibrator, while a value of 3.3 corresponds to the case of a rigid rotor. In Fig. 5 the experimental  $B_{4/2}$  and  $R_{4/2}$  ratios for six even Pd isotopes are shown in black. Red points mark ratios calculated with the SR88MHJM interaction. By increasing the number of valence neutrons outside the closed  $N = 50$  shell, the experimental  $R_{4/2}$  ratio increases beyond the vibrational value of 2, reaches a maximum of 2.38 at  $^{104}\text{Pd}$  and a value of 2.15 at  $^{106}\text{Pd}$ . The shell-model calculation follows the experimental results. Experimentally,  $^{104}\text{Pd}$  has

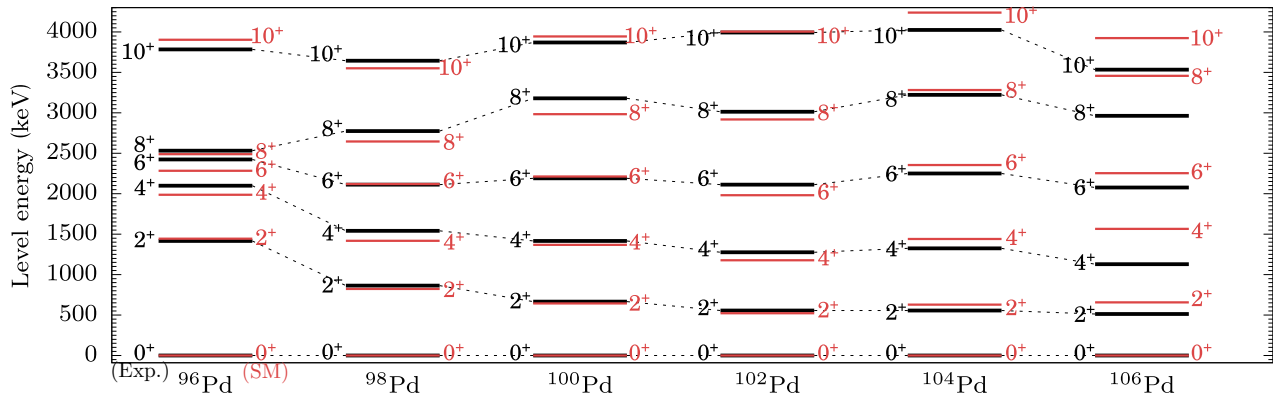


FIG. 6. Experimental excitation energies (black) for even-even palladium isotopes of the positive-parity ground-state band up to the  $10^+$  state, starting from the  $N = 50$  shell closure up to the midshell  $N = 60$  nucleus  $^{106}\text{Pd}$ , compared with the calculated values using the SR88MHJM interaction (red).

the highest  $R_{4/2}$  value of the given  $Z = 46$  isotopes. The ratio of the reduced transition strengths  $B_{4/2}$  is expected to be larger than one for collective nuclei [40,41]. In the collective model of Bohr and Mottelson [42], a deformed rotating nucleus is characterised by  $B_{4/2}(\text{rot.}) \approx 1.43$ , whereas a vibrational motion by  $B_{4/2}(\text{vib.}) = 2$ . Starting from single particle excitations at the  $N = 50$  shell closure, the  $B_{4/2}$  ratios increase and approach values consistent with a collective character of the excited states. Beyond  $^{100}\text{Pd}$  the  $B_{4/2}$  ratio for medium-mass Pd isotopes stays nearly constant and agrees with rotor properties. Known experimental results as well as shell-model calculations agree well also for the  $B_{4/2}$  ratios.

Thus, while the  $R_{4/2}$  ratios indicate vibrator properties, the  $B_{4/2}$  ratio is closer to rotor values and the simplified vibrator or rotor picture does not reproduce the structure of the ground-state band in  $^{104}\text{Pd}$ . The SR88MHJM calculation, however, reflects the ambiguous behavior of the  $^{96-106}\text{Pd}$  isotope chain.

The emergence of quadrupole collectivity in nuclei has been successfully described by shell-model calculations for light nuclei with a quasi-SU(3) symmetry [43] while for heavier nuclei quasi- and pseudo-SU(3) symmetries play a role as shown in Ref. [44]. This was recently demonstrated for the light Sn and Cd isotopes by Zuker [45].

By reproducing the known experimental  $B(E2; 2_1^+ \rightarrow 0_{\text{g.s.}}^+)$  and  $B(E2; 4_1^+ \rightarrow 2_1^+)$  transitions in the light Cd isotopes for  $N \leq 62$  that paper showed that the shell-model calculations can have a nearly perfect agreement with the Alaga rule value  $B_{4/2} = 1.43$ , which is similar with the result of our calculations for the light ( $N \leq 60$ ) Pd isotopes (see Fig. 5).

The good reproduction of a vibrational type of spectrum in the light Pd isotopes can be understood by comparing to previous SM results for neighboring Cd isotopes. The recent shell-model description of these isotopes, with an interaction similar to the SR88MHJM, included a theoretical deformation analysis of the lowest yrast states [46]. For the ground state the SM values of  $\beta$  and  $\gamma$  deformation parameters have shown increasing deformation and triaxiality with increasing number of valence neutrons [46].

A similar result emerged for the neighboring light Sn isotopes from a more advanced large-scale MCSM study of the Sn isotopes, where the T plots for  $^{104,108}\text{Sn}$  clearly show

triaxial deformation [47]. These findings support a picture of the light Cd isotopes as a  $\gamma$  soft or even more complex nuclei, opposite to the pure vibrational picture. In the view of the above, a similar behavior for some light Pd isotopes (including isotope  $^{104}\text{Pd}$ ) can be considered. The good reproduction of the experimental  $R_{4/2}$  and  $B_{4/2}$  by the shell-model calculations presented in this work is attributed on one side to the quality of the Hamiltonian and on the other side to the large-enough model space containing the relevant proton and neutron single-particle orbitals to introduce pseudo- and quasi-SU(3) quadrupole collectivity (see Ref. [45]) as well as single-particle excitations.

In Fig. 6 the calculations are shown and compared with experimental ground-state band for states up to  $10^+$ . In general, excitation energies are well reproduced by the shell-model calculation. Up to  $^{102}\text{Pd}$  the systematics is nicely reproduced; the excitation energy of the first two excited states decreases with increasing neutron number. At the  $N = 56$  isotope  $^{102}\text{Pd}$ , the shell-model calculations show a minimum of the excitation energies up to the  $6_1^+$  state. The experimental excitation energies of the  $2_1^+$  and  $4_1^+$  states and to some extent of the  $6_1^+$  state from  $^{96}\text{Pd}$  to  $^{104}\text{Pd}$  shows a parabolic trend suggesting slowly filling orbitals and no distinct subshell closure.

The close-lying, with respect to the SPE,  $2d_{5/2}$  and  $1g_{7/2}$  neutron orbitals seem to be filled simultaneously as suggested by the occupation numbers calculated by SM for both orbitals. A similar effect was already shown and discussed for light  $^{99-111}\text{Cd}$  isotopes using the same SM interaction [31]. The excitation energies of the ground-state band are best reproduced for  $^{100}\text{Pd}$  with a mean deviation of 88 keV. The calculated excitation energies in the ground-state band for  $^{104}\text{Pd}$  also show good agreement with a mean deviation of 125 keV, while for  $^{106}\text{Pd}$  there is a discrepancy with a mean deviation of 358 keV.

The increase in collectivity in the light Pd nuclei, already demonstrated by the  $R_{4/2}$  behavior, is also reflected by the increasing electric quadrupole transition strengths between the low-lying yrast states. This behavior is correctly reproduced by the SR88MHJM calculation up to  $^{104}\text{Pd}$ . Figure 7 shows the experimental (black) and theoretical (red)

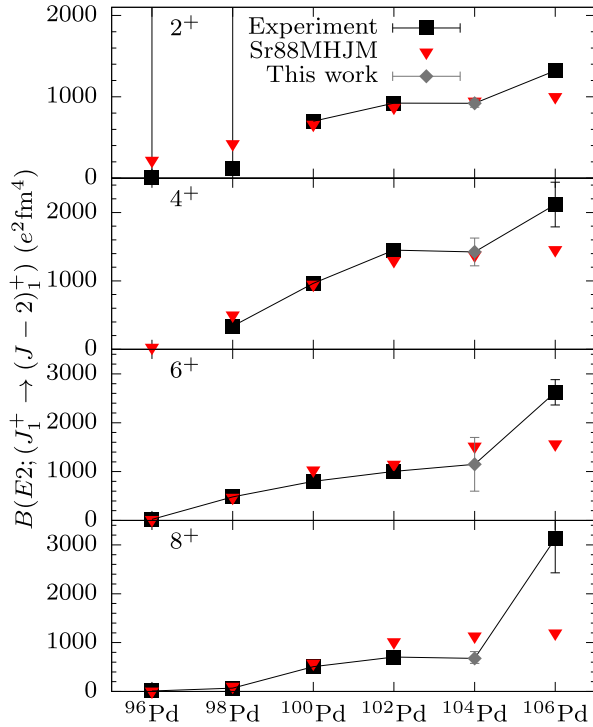


FIG. 7. Experimental transition strengths (black) for even-even palladium isotopes  $^{96-106}\text{Pd}$ , compared with the calculated values using the SR88MHJM interaction (red). Only lower limits are known for transition strengths of the  $2_1^+$  state in the lightest calculated isotopes.

transition strength values up to the  $8_1^+$  state in the positive-parity ground-state band. While most experimental values for  $J_1^+ \geq 10_1^+$  states are missing, the comparison is limited to yrast states up to the  $8^+$  state. New values for  $^{104}\text{Pd}$  are marked in gray.

Discrepancies between the calculated and experimental  $B(E2)$  values are found for  $^{106}\text{Pd}$  where the experimental values are suddenly increased especially for states with higher spins. The experimental transition strength values of ground-state band transitions in  $^{96-104}\text{Pd}$  show highest  $B(E2)$  values for the  $2_1 \rightarrow 0_{\text{g.s.}}$  and  $4_1 \rightarrow 2_1$  transitions, while the  $B(E2)$  values stay constant or are even get smaller for higher spin values. For  $^{106}\text{Pd}$ , the experimental transition probabilities increase continuously as a function of spin. In comparison with experimental values, all theoretical  $^{106}\text{Pd}$  values are too low with experimental values which are similar to neighboring  $^{104}\text{Pd}$ .

### B. Shell-model calculations of high-spin states in $^{104}\text{Pd}$

In order to compare all existing experimental findings for the yrast band in  $^{104}\text{Pd}$  with shell-model theory, the excitation energies and  $B(E2)$  values were calculated up to a spin of  $J^\pi = 26^+\hbar$  employing the SR88MHJM interaction. A comparison between the SM and experimental data is shown in Fig. 8. The calculated transition energies (e.g., differences in energy of the corresponding levels) and transition strengths are shown in red triangles, experimental values are marked

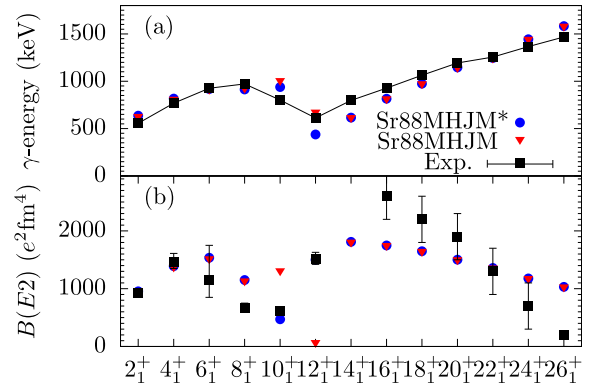


FIG. 8. Experimental and calculated (a) transition energies and (b) transition strength values. Results of the SR88MHJM interaction are shown in red triangles. Results with reduced  $\nu h_{11/2}$  SPE (SR88MHJM\*) are shown in blue circles. See text for more details.

with black squares. Results of low-spin states  $J^\pi \leq 12^+\hbar$  are furthermore given in Table I.

The calculated transition energies of low-spin states  $J^\pi \leq 8^+$  are in good agreement with the adopted values. While the transition energies of the  $10_1^+ \rightarrow 8_1^+$  and  $12_1^+ \rightarrow 10_1^+$  transitions are slightly overestimated by the SR88MHJM interaction, the  $14_1^+ \rightarrow 12_1^+$  transition energy is underestimated. The calculated transition energies do not reproduce the experimentally observed minimum at the  $12_1^+ \rightarrow 10_1^+$  transition. Starting from the  $14_1^+ \rightarrow 12_1^+$  transition up to  $26_1^+ \rightarrow 24_1^+$ , the nearly linear experimental increase is reflected by theory but with a different slope.

Similarly to the transition energies, the theoretical  $B(E2; 2_1^+ \rightarrow 0_{\text{g.s.}})$  and  $B(E2; 4_1^+ \rightarrow 2_1^+)$  values are in excellent agreement with the new experimental values. The  $6_1^+ \rightarrow 4_1^+$  transition strength was determined with large uncertainty and the calculation agrees within the errors. The decreasing transition strength toward the  $8_1^+ \rightarrow 6_1^+$  transition is correctly reproduced by shell-model theory, but experimental values of  $B(E2; 8_1^+ \rightarrow 6_1^+)$  and  $B(E2; 10_1^+ \rightarrow 8_1^+)$  deviate clearly from theory. A huge discrepancy occurs at the  $B(E2; 12_1^+ \rightarrow 10_1^+)$  value. Here the SR88MHJM yields an isomeric state with  $B(E2; 12_1^+ \rightarrow 10_1^+) = 68 e^2 \text{fm}^4$ , whereas the measured value  $B(E2; 12_1^+ \rightarrow 10_1^+) = 1520_{-100}^{+110} e^2 \text{fm}^4$  is much larger. From the  $16_1^+ \rightarrow 14_1^+$  transition onwards the experimental transition strength values decrease almost linearly as a function of angular momentum. Although the SM underestimates the  $16_1^+ \rightarrow 14_1^+$  transition strength it reproduces the linear decrease but with a smaller slope.

In order to understand the considerable discrepancies between the experimental and calculated results for  $B(E2; 10_1^+ \rightarrow 8_1^+)$  and  $B(E2; 12_1^+ \rightarrow 10_1^+)$  values, the shell-model description is studied in more detail. The calculated second  $10_2^+$  state is found to be only 234 keV above the  $10_1^+$  state in excitation energy. Moreover, the corresponding SR88MHJM value of  $B(E2; 12_1^+ \rightarrow 10_2^+) = 1732 e^2 \text{fm}^4$  value is very close to the experimental value of  $B(E2; 12_1^+ \rightarrow 10_1^+) = 1520_{-100}^{+110} e^2 \text{fm}^4$ . It is intriguing to assume that calculated  $10_1^+$  and  $10_2^+$  states are interchanged. This hypothesis

TABLE II. Occupation numbers of  $8_1^+$ ,  $10_1^+$ ,  $10_2^+$ , and  $12_1^+$  states in  $^{104}\text{Pd}$  calculated using the original (top) interaction and the calculation with reduced  $\nu h_{11/2}$  SPE by 200 keV (bottom) labeled with an asterisk.

SR88MHJM	$\pi p_{1/2}$	$\pi g_{9/2}$	$\nu d_{5/2}$	$\nu g_{7/2}$	$\nu d_{3/2}$	$\nu s_{1/2}$	$\nu h_{11/2}$
$8_1^+$	6.18	1.82	2.48	3.59	0.86	0.56	0.52
$10_1^+$	6.13	1.87	2.34	3.62	0.84	0.62	<b>0.58</b>
$10_2^+$	6.18	1.82	2.29	2.69	0.67	0.39	<b>1.96</b>
$12_1^+$	6.13	1.87	2.27	2.63	0.68	0.39	2.03
SR88MHJM*	$\pi p_{1/2}$	$\pi g_{9/2}$	$\nu d_{5/2}$	$\nu g_{7/2}$	$\nu d_{3/2}$	$\nu s_{1/2}$	$\nu h_{11/2}$
$8_1^+$	6.18	1.82	2.44	3.51	0.84	0.54	0.67
$10_1^+$	6.11	1.89	2.29	2.78	0.70	0.43	<b>1.79</b>
$10_2^+$	6.16	1.84	2.32	3.38	0.80	0.56	<b>0.95</b>
$12_1^+$	6.13	1.87	2.26	2.63	0.68	0.39	2.05

is further corroborated by the calculated occupation numbers which are shown for the  $8_1^+$ ,  $10_1^+$ ,  $10_2^+$ , and  $12_1^+$  states in the upper part of Table II. Results of the SR88MHJM interaction show an  $h_{11/2}^2$  character for the  $12_1^+$  and  $10_2^+$  states which is not the case for the  $10_1^+$  state.

The SPE energy of the  $\nu h_{11/2}$  orbital was scrutinised to resolve the obvious change of wave-function content between the two neighboring  $10^+$  states. Due to the  $\nu h_{11/2}^2$  character of the  $10_2^+$  state, a reduction of the  $h_{11/2}$  SPE lowers the excitation energy of the  $10_2^+$  state. In this way the sequence of the two  $10^+$  states will be interchanged and both observables, excitation energy and  $B(E2)$  value, will be in much better agreement with the experiment.

For a quantitative study of the suggested shift of the  $\nu h_{11/2}$  SPE, single-particle  $11/2^-$  states were calculated also for the two neighboring even-odd Pd isotopes  $^{103,105}\text{Pd}$ . The SR88MHJM results overestimate the experimental excitation energies of these single neutron states by  $\approx 200$  keV in both isotopes, supporting again the reduction of the  $\nu h_{11/2}$  SPE for an improved description of  $^{104}\text{Pd}$ . On the one side, this could be an effect of improper monopole shift of the  $\nu h_{11/2}$  orbital realized by monopole terms in the two-body matrix elements. And on the other side, such a lowering of the  $\nu h_{11/2}$  SPE could probably be related to increased deformation when approaching  $N = 60$  and the down sloping of high- $j$  orbitals, which is beyond the frame of the spherical-based interacting shell-model applied in this work. New calculations were then performed in  $^{104}\text{Pd}$  by modifying within the SR88MHJM interaction solely the  $\nu h_{11/2}$  SPE. The deviations between experimental and calculated  $B(E2; 12_1^+ \rightarrow 10_1^+)$ ,  $B(E2; 10_1^+ \rightarrow 8_1^+)$ , and  $B(E2; 8_1^+ \rightarrow 6_1^+)$  values were studied as a function of the  $\nu h_{11/2}$  SPE shift. Best overall agreement was obtained after a reduction of the  $\nu h_{11/2}$  SPE by 200 keV.

Some results of the modified interaction, denoted by SR88MHJM\*, are shown first in the lower part of Table II, where the wave-function content with respect to the  $\nu h_{11/2}$  orbital is exchanged between the  $10_1^+$  and  $10_2^+$  states (highlighted with bold). Other wave functions and their occupation numbers have barely changed after this modification. The calculated transition energies and transition strength values of the yrast band using the modified SR88MHJM\* interaction are shown in Fig. 8 and in Table I up to  $J^\pi = 12^+\hbar$ . The mod-

ifications cause in most cases improvements of the transition energies. The position of the transition energy minimum is now correctly reproduced at the  $12^+ \rightarrow 10^+$  transition. A significant improvement was achieved for the  $B(E2; 10_1^+ \rightarrow 8_1^+)$  and  $B(E2; 12_1^+ \rightarrow 10_1^+)$  values reproducing the experimental findings for the  $10_1^+$  and  $12_1^+$  state convincingly, while other states remain unaffected by the modifications. Altogether, the reproduction of the yrast band transition energies and strengths suggests that the character of the yrast band starting from the  $10_1^+$  is based on  $\nu h_{11/2}^2$  excitation.

## VI. SUMMARY

The fusion-evaporation reaction  $^{96}\text{Zr}(^{12}\text{C}, 4n)^{104}\text{Pd}$  was used to perform precise lifetime measurements of excited states in  $^{104}\text{Pd}$  employing the Cologne plunger and the RDDS method. Lifetimes of the first six states of the ground-state band were determined, four of them for the very first time. The lifetime of the  $2_1^+$  state corresponds to a reduced transition strength  $B(E2; 2_1^+ \rightarrow 0_{g.s.}^+) = 31.9_{-1.6}^{+1.8}$  W.u. that is well below the adopted value  $B(E2; 2_1^+ \rightarrow 0_{g.s.}^+) = 36.4(10)$  W.u. [8] deduced from Coulex and electron scattering data. This new value can impact results of Coulex measurements in which  $^{104}\text{Pd}$   $B(E2; 2_1^+ \rightarrow 0_{g.s.}^+)$  is used for normalisation, for example being the scattering target of radioactive ion beams.

New LSSM calculations were performed employing the SR88MHJM interaction in the light even-even isotope chain from  $^{96}\text{Pd}$  at the  $N = 50$  shell closure up to  $^{106}\text{Pd}$ . The results show good agreement for the excitation energies and  $B(E2)$  values of low-lying  $J_1^+ \leq 8_1^+$  states for the isotopes up to  $^{104}\text{Pd}$ . Clear deviations are observed for  $^{106}\text{Pd}$  where the calculated values are smaller than the experimental transition strength values. The sudden increase in  $E2$  strength from  $N = 58$  to  $N = 60$  nuclei is observed in other  $Z \leq 46$  isotope chains, e.g., the  $Z = 40$  zirconium chain where it is understood as a phase transition between nearly spherical to deformed nuclei [48]. A starting deformation in the  $N = 60$  palladium isotopes was already suggested by lifetime measurements in odd palladium isotopes by Bucher *et al.* [49] in 2015 and it is in line with results of the present study. In the palladium chain, a gradual increase in transition strengths between the  $N = 58$  and  $N = 60$  nuclei  $^{104}\text{Pd}$  and  $^{106}\text{Pd}$  is

observed. From the experimental and calculated ratios of  $4_1^+$  and  $2_1^+$  excitation energies ( $R_{4/2}$ ) and transition strengths ( $B_{4/2}$ ), a vibrator-like behavior is found in terms of the excitation energy while the rotorlike values are consistent with the transition strength ratios of even-even  $^{98-106}\text{Pd}$ .

To learn more from the successful shell model reproduction of the  $B_{4/2}$  and  $R_{4/2}$  ratios in the light Pd chain, a shell model based deformation analysis similar to Ref. [46] suggests itself also for these isotopes in the near future.

The higher-spin states up to  $J_1^+ = 26_1^+$  were subject of a dedicated shell-model analysis and comparison to experimental data including our results and latest findings by [18,20]. The original SR88MHJM results yielded deviations for the excitation energies of the  $J_1^+ = 10_1^+$  and  $J_1^+ = 12_1^+$  states and considerable discrepancies for the  $B(E2; 10_1^+ \rightarrow 8_1^+)$  and  $B(E2; 12_1^+ \rightarrow 10_1^+)$  values. Especially, the very small  $B(E2; 12_1^+ \rightarrow 10_1^+)$  value did not comply with the measured value. The difference between the experimental and calculated results was traced down to the  $h_{11/2}$  SPE and the wave functions of adjacent neighboring  $J_i^+ = 10^+$  states. Finally, a justified

ad-hoc modification of the  $h_{11/2}$  SPE for calculations of  $^{104}\text{Pd}$  with the SR88MHJM interaction resolved the discrepancies and reproduced the experimental  $B(E2)$  values satisfactorily.

In future, the sudden increase in collectivity at  $^{106}\text{Pd}$ , which could not be reproduced by the new LSSM calculation, should be investigated further. Especially, the  $B(E2; 8_1^+ \rightarrow 6_1^+)$  value is not reproduced by the shell-model results. This value was determined once by Svensson *et al.* in Ref. [50]. Remeasuring this value together with the transition strength of higher spin states in  $^{106}\text{Pd}$  is desirable. Moreover, lifetime measurements combined with shell-model calculations along the isotonic chain, e.g., for  $^{106}\text{Cd}$  and  $^{102}\text{Ru}$ , where the  $B(E2; 10^+ \rightarrow 8^+)$  and  $B(E2; 12^+ \rightarrow 10^+)$  values are not known, or only with large error, are of high interest.

#### ACKNOWLEDGMENT

We thank the IKP FN tandem accelerator team for the excellent support during the experiment.

- 
- [1] D. J. Rowe and J. L. Wood, *Fundamentals of Nuclear Models: Foundational Models* (World Scientific, Singapore, 2010).
- [2] C. Fransen (private communication).
- [3] V. Anagnostatou, P. H. Regan, M. R. Bunce, D. McCarthy, V. Werner, T. Ahn, R. J. Casperson, R. Chevri er, N. C. A. Heinz, G. Ilie, M. K. Smith, E. Williams, L. Bettermann, D. Radeck, C. W. Beausang, C. Boniwell, and B. Pauerstein, Measurements of picosecond lifetimes in the transitional nucleus  $^{100}\text{Pd}$  using the RDDM in inverse kinematics, *Acta Phys. Pol. B* **42**, 807 (2011).
- [4] D. Radeck, A. Blazhev, M. Albers, C. Bernards, A. Dewald, C. Fransen, M. Heidemann, J. Jolie, B. Melon, D. M ucher, T. Pissulla, W. Rother, K. O. Zell, and O. M oller, First measurement of lifetimes in the Yrast band of  $^{100}\text{Pd}$ , *Phys. Rev. C* **80**, 044331 (2009).
- [5] T. Konstantinopoulos, S. F. Ashley, M. Axiotis, A. Spyrou, S. Harissopolos, A. Dewald, J. Litzinger, O. M oller, C. M uller-Gaterman, P. Petkov, D. R. Napoli, N. Marginean, G. de Angelis, C. A. Ur, D. Bazzacco, E. Farnea, S. M. Lenzi, R. Vlastou, and D. Balabanski, Lifetime measurements in  $^{102}\text{Pd}$ : Searching for empirical proof of the E(5) critical-point symmetry in nuclear structure, *Phys. Rev. C* **93**, 014320 (2016).
- [6] E. Peters, F. Prados-Est vez, A. Chakraborty, M. Mynk, D. Bandyopadhyay, S. Choudry, B. Crider, P. Garrett, S. Hicks, A. Kumar, S. R. Leshner, C. J. McKay, J. N. Orce, M. Scheck, J. R. Vanhoy, J. L. Wood, and S. W. Yates, E0 transitions in  $^{106}\text{Pd}$ : Implications for shape coexistence, *Eur. Phys. J. A* **52**, 96 (2016).
- [7] G. G urdal, G. J. Kumbartzki, N. Benczer-Koller, Y. Y. Sharon, L. Zamick, S. J. Q. Robinson, T. Ahn, R. Casperson, A. Heinz, G. Ilie, J. Qian, V. Werner, E. Williams, R. Winkler, and D. McCarthy,  $g$  factors of the low-lying states in  $^{106}\text{Pd}$ : Examination of the vibrational character of  $^{106}\text{Pd}$ , *Phys. Rev. C* **82**, 064301 (2010).
- [8] B. Pritychenko, M. Birch, B. Singh, and M. Horoi, Tables of E2 transition probabilities from the first  $2^+$  states in even-even nuclei, *At. Data Nucl. Data Tables* **107**, 1 (2016).
- [9] G. M. Temmer and N. P. Heydenburg, Coulomb excitation of medium-weight nuclei, *Phys. Rev.* **104**, 967 (1956).
- [10] P. H. Stelson and F. K. McGowan, Coulomb excitation of medium-weight even-even nuclei, *Phys. Rev.* **110**, 489 (1958).
- [11] K. Alder, A. Bohr, T. Huus, B. Mottelson, and A. Winther, Study of nuclear structure by electromagnetic excitation with accelerated ions, *Rev. Mod. Phys.* **28**, 432 (1956).
- [12] T. Czosnyka, D. Cline, and C. Y. Wu, Coulomb excitation data analysis code GOSIA, *Bull. Am. Phys. Soc.* **28**, 745 (1983).
- [13] M. Zieli nska, L. P. Gaffney, K. Wrzosek-Lipska, E. Cl ement, T. Grahn, N. Kesteloot, P. Napiorkowski, J. Pakarinen, P. Van Duppen, and N. Warr, Analysis methods of safe Coulomb-excitation experiments with radioactive ion beams using the GOSIA code, *Eur. Phys. J. A* **52**, 99 (2016).
- [14] A. Christy, I. Hall, R. P. Harper, I. M. Naqib, and B. Wakefield, Measurement of the static quadrupole moments of the first  $2^+$  states in  $^{104,106}\text{Pd}$  and  $^{130}\text{Te}$ , *Nucl. Phys. A* **142**, 591 (1970).
- [15] K. Alder and A. Winther, *Coulomb Excitation: A Collection of Reprints* (Academic Press, New York, 1966).
- [16] J. Wesseling, C. W. de Jager, J. B. V. D. Laan, H. D. Vries, and M. N. Harakeh, IBA  $g$ -boson properties in  $^{110}\text{Cd}$  and Pd isotopes studied with electron scattering, *Nucl. Phys. A* **535**, 285 (1991).
- [17] M. Luontama, R. Julin, J. Kantele, A. Passoja, W. Trzaska, A. B acklin, N.-G. Jonsson, and L. Westerberg, Electromagnetic properties of low-spin states in  $^{102,104}\text{Pd}$ , *Z. Phys.* **3**, 317 (1986).
- [18] N. Rather, S. Roy, P. Datta, S. Chattopadhyay, A. Goswami, S. Nag, R. Palit, S. Pal, S. Saha, J. Sethi, T. Trivedi, and H. C. Jain, Antimagnetic rotation in  $^{104}\text{Pd}$ , *Phys. Rev. C* **89**, 061303(R) (2014).
- [19] S. Frauendorf, Tilted cranking, *Nucl. Phys. A* **557**, 259 (1993).
- [20] C. Majumder, H. P. Sharma, S. Chakraborty, S. S. Tiwary, R. P. Singh, S. Muralithar, I. Bala, S. S. Bhattacharjee, R. Garg, Neelam, A. Sharma, and P. V. M. Rao, Lifetime

- measurements in  $^{104}\text{Pd}$ , *J. Phys. G: Nucl. Part. Phys.* **47**, 125104 (2020).
- [21] D. Sohler, I. Kuti, J. Timár, P. Joshi, J. Molnár, E. S. Paul, K. Starosta, R. Wadsworth, A. Algora, P. Bednarczyk, D. Curien, Z. Dombrádi, G. Duchene, D. B. Fossan, J. Gál, A. Gizon, J. Gizon, D. G. Jenkins, K. Juhász, G. Kalinka *et al.*, High-spin structure of  $^{104}\text{Pd}$ , *Phys. Rev. C* **85**, 044303 (2012).
- [22] D. Ivanova, S. Lalkovski, C. Costache, S. Kisiov, C. Mihai, N. Mrginean, P. Petkov, L. Atanasova, D. Bucurescu, R. B. Cakirli, M. P. Carpenter, R. F. Casten, G. Cta-Danil, I. Cta-Danil, D. Deleanu, D. Filipescu, N. Florea, I. Gheorghe, D. Ghiț, T. Glodariu *et al.*, Structure of the low-lying states in  $^{99,101,103,105}\text{Pd}$ , *Phys. Rev. C* **105**, 034337 (2022).
- [23] V. Devi, Structure and odd–even staggering of Mo, Ru, and Pd even–even nuclei in the framework of IBM-1, *Turk. J. Phys.* **37**, 330 (2013).
- [24] A. Giannatiempo, Vibrational- $\gamma$  bands in even  $^{104-118}\text{Pd}$  isotopes, *Phys. Rev. C* **98**, 034305 (2018).
- [25] Z.-H. Zhang, Theoretical investigation of the antimagnetic rotation in  $^{104}\text{Pd}$ , *Chin. Phys. C* **43**, 054107 (2019).
- [26] N. Shimizu, T. Mizusaki, Y. Utsuno, and Y. Tsunoda, Thick-restart block Lanczos method for large-scale shell-model calculations, *Comput. Phys. Commun.* **244**, 372 (2019).
- [27] O. Kavatsyuk, C. Mazzocchi, Z. Janas, A. Banu, L. Batist, F. Becker, A. Blazhev, W. Brüche, J. Döring, T. Faestermann, M. Górska, H. Grawe, A. Jungclaus, M. Karny, M. Kavatsyuk, O. Klepper, R. Kirchner, M. La Commara, K. Miernik, I. Mukha *et al.*, Beta decay of  $^{101}\text{Sn}$ , *Eur. Phys. J. A* **31**, 319 (2007).
- [28] T. Faestermann, M. Górska, and H. Grawe, The structure of  $^{100}\text{Sn}$  and neighbouring nuclei, *Prog. Part. Nucl. Phys.* **69**, 85 (2013).
- [29] B. J. Coombes, A. E. Stuchbery, A. Blazhev, H. Grawe, M. W. Reed, A. Akber, J. T. H. Dowie, M. S. M. Gerathy, T. J. Gray, T. Kibédi, A. J. Mitchell, and T. Palazzo, Spectroscopy and excited-state  $g$  factors in weakly collective  $^{111}\text{Cd}$ : Confronting collective and microscopic models, *Phys. Rev. C* **100**, 024322 (2019).
- [30] J. Park, R. Krücken, D. Lubos, R. Gernhäuser, M. Lewitowicz, S. Nishimura, D. S. Ahn, H. Baba, B. Blank, A. Blazhev, P. Boutachkov, F. Browne, I. Čeliković, G. de France, P. Doornenbal, T. Faestermann, Y. Fang, N. Fukuda, J. Giovinazzo, N. Goel *et al.*, Properties of  $\gamma$ -decaying isomers and isomeric ratios in the  $^{100}\text{Sn}$  region, *Phys. Rev. C* **96**, 044311 (2017).
- [31] D. T. Yordanov, D. L. Balabanski, M. L. Bissell, K. Blaum, A. Blazhev, I. Budinčević, N. Frömmgen, C. Geppert, H. Grawe, M. Hammen, K. Kreim, R. Neugart, G. Neyens, and W. Nörtershäuser, Spins and electromagnetic moments of  $^{101-109}\text{Cd}$ , *Phys. Rev. C* **98**, 011303(R) (2018).
- [32] H. Grawe, K. Straub, T. Faestermann, M. Górska, C. Hinke, R. Krücken, F. Nowacki, M. Böhmer, P. Boutachkov, H. Geissel, R. Gernhäuser, A. Gottardo, J. Grbosz, N. Kurz, Z. Liu, L. Maier, S. Pietri, Z. Podolyák, K. Steiger, H. Weick *et al.*, The  $(6^+)$  isomer in  $^{102}\text{Sn}$  revisited: Neutron and proton effective charges close to the double shell closure, *Phys. Lett. B* **820**, 136591 (2021).
- [33] A. Dewald, O. Möller, and P. Petkov, Developing the Recoil Distance Doppler-Shift technique towards a versatile tool for lifetime measurements of excited nuclear states, *Prog. Part. Nucl. Phys.* **67**, 786 (2012).
- [34] A. Dewald, S. Harissopulos, and P. von Brentano, The differential plunger and the differential decay curve method for the analysis of recoil distance Doppler-shift data, *Z. Physik A - Atomic Nuclei* **334**, 163 (1989).
- [35] K. Arnsward, T. Braunroth, M. Seidlitz, L. Coraggio, P. Reiter, B. Birkenbach, A. Blazhev, A. Dewald, C. Fransen, B. Fu, A. Gargano, H. Hess, R. Hirsch, N. Itaco, S. M. Lenzi, L. Lewandowski, J. Litzinger, C. Müller-Gatermann, M. Queiser, D. Rosiak *et al.*, Enhanced collectivity along the  $N = Z$  line: Lifetime measurements in  $^{44}\text{Ti}$ ,  $^{48}\text{Cr}$ , and  $^{52}\text{Fe}$ , *Phys. Lett. B* **772**, 599 (2017).
- [36] L. Barber, D. M. Cullen, M. M. Giles, B. S. Nara Singh, M. J. Mallaburn, M. Beckers, A. Blazhev, T. Braunroth, A. Dewald, C. Fransen, A. Goldkuhle, J. Jolie, F. Mammes, C. Müller-Gatermann, D. Wölk, and K. Zell, Performing the differential decay curve method on  $\gamma$ -ray transitions with unresolved Doppler-shifted components, *Nucl. Instrum. Methods A* **950**, 162965 (2020).
- [37] P. Petkov, J. Gableske, O. Vogel, A. Dewald, P. von Brentano, R. Krücken, R. Peusquens, N. Nicolay, A. Gizon, J. Gizon, D. Bazzacco, C. Rossi-Alvarez, S. Lunardi, P. Pavan, D. R. Napoli, W. Andrejtscheff, and R. Jolos, In-band M1 and E2 transition rates and collective structures in  $^{128}\text{Ba}$ , *Nucl. Phys. A* **640**, 293 (1998).
- [38] P. Petkov, D. Tonev, J. Gableske, A. Dewald, T. Klemme, and P. von Brentano, On the line-shape and lifetime determination in recoil distance Doppler-shift measurements, *Nucl. Instrum. Methods A* **431**, 208 (1999).
- [39] T. Klemme, A. Fitzler, A. Dewald, S. Schell, S. Kasemann, R. Kühn, O. Stuch, H. Tiesler, K. O. Zell, P. von Brentano, D. Bazzacco, F. Brandolini, S. Lunardi, C. M. Petrache, C. Rossi Alvarez, G. De Angelis, P. Petkov, and R. Wyss, Lifetimes measurements for  $^{134}\text{Nd}$  and neighboring nuclei with the coincidence-plunger technique, *Phys. Rev. C* **60**, 034301 (1999).
- [40] S. M. Lenzi, E. E. Maqueda, and P. Von Brentano, E2 transitions in the SU(3) formalism for  $N=Z$  nuclei of the sd and pf shells. *The European Physical Journal A-Hadrons and Nuclei* **27**, 341 (2006).
- [41] R. B. Cakirli, R. F. Casten, J. Jolie, and N. Warr, Highly anomalous yrast  $B(E2)$  values and vibrational collectivity, *Phys. Rev. C* **70**, 047302 (2004).
- [42] A. Bohr and B. R. Mottelson, *Nuclear Structure*, Vol. 2, Nuclear Deformations (World Scientific Publishing, New York, 1975).
- [43] A. P. Zuker, J. Retamosa, A. Poves, and E. Caurier, Spherical shell model description of rotational motion, *Phys. Rev. C* **52**, R1741 (1995).
- [44] E. Caurier, G. Martínez-Pinedo, F. Nowacki, A. Poves, and A. P. Zuker, The shell model as a unified view of nuclear structure, *Rev. Mod. Phys.* **77**, 427 (2005).
- [45] A. P. Zuker, Quadrupole dominance in the light sn and in the cd isotopes, *Phys. Rev. C* **103**, 024322 (2021).
- [46] T. Schmidt, K. L. G. Heyde, A. Blazhev, and J. Jolie, Shell-model-based deformation analysis of light cadmium isotopes, *Phys. Rev. C* **96**, 014302 (2017).
- [47] T. Togashi, Y. Tsunoda, T. Otsuka, N. Shimizu, and M. Honma, Novel Shape Evolution in sn Isotopes from

- Magic Numbers 50 to 82, [Phys. Rev. Lett. \*\*121\*\*, 062501 \(2018\)](#).
- [48] V. Karayonchev, J. Jolie, A. Blazhev, A. Dewald, A. Esmaylzadeh, C. Fransen, G. Häfner, L. Knafla, J. Litzinger, C. Müller-Gatermann, J.-M. Régis, K. Schomacker, A. Vogt, N. Warr, A. Leviatan, and N. Gavrielov, Tests of collectivity in  $^{98}\text{Zr}$  by absolute transition rates, [Phys. Rev. C \*\*102\*\*, 064314 \(2020\)](#).
- [49] B. Bucher, H. Mach, A. Aprahamian, G. S. Simpson, J. Rissanen, D. G. Ghiță, B. Olaizola, W. Kurcewicz, J. Äystö, I. Bentley, T. Eronen, L. M. Fraile, A. Jokinen, P. Karvonen, I. D. Moore, H. Penttilä, M. Reponen, E. Ruchowska, A. Saastamoinen, M. K. Smith *et al.*, New lifetime measurements in  $^{109}\text{Pd}$  and the onset of deformation at  $N = 60$ , [Phys. Rev. C \*\*92\*\*, 064312 \(2015\)](#).
- [50] L. E. Svensson, C. Fahlander, L. Hasselgren, A. Bäcklin, L. Westerberg, D. Cline, T. Czosnyka, C. Y. Wu, R. M. Diamond, and H. Kluge, Multiphonon vibrational states in  $^{106,108}\text{Pd}$ , [Nucl. Phys. A \*\*584\*\*, 547 \(1995\)](#).